ISSN: 2348 - 2117

International Journal of Engineering Technology and Computer Research (IJETCR)
Available Online at www.ijetcr.org
Volume 5; Issue 5; September-October: 2017; Page No. 35-49
Journal Approved by UGC

Flow boiling heat transfer performance of eco-friendly refrigerants

Arijit Kundu

Department of Mechanical Engineering, Jalpaiguri Government Engineering College, Jalpaiguri, West Bengal, India 735102

arijit.kundu@me.jgec.ac.in

Received 16 Aug. 2017; Accepted 08 Sep. 2017

Abstract

An experimental investigation of the flow boiling heat transfer for eco-friendly pure refrigerant (R600a) and quasi-azeotropic mixture (R410A) has been presented. The test section is a smooth horizontal tube (7 mm ID) uniformly heated by the resistance heating effect. The flow boiling characteristics of the refrigerant fluids are evaluated varying the refrigerant mass flux within the range of 100-400 kg/m^{2}s, the heat fluxes within the range 3.0-10.0 kW/m^2; inlet temperatures to the evaporator are maintained within 5^{o}C-9^{o}C. In this study, the effect of vapor quality, mass flux, imposed heat flux and fluid thermo-physical properties of the heat transfer coefficient and two-phase pressure drop are examined. Moreover, an assessment of predictive methods is provided for local heat transfer coefficients; also a comparison of flow regimes visualizations for R600a and R410A with a flow pattern map available in the literature is presented.

Key Words: flow boiling, heat transfer coefficient, pressure drop, flow pattern map, R600a, R410A.

NOMENCLATURE

AN active nucleation sites (K-N-m/J/kg-kg/m^3)
C_P specific heat at constant pressure (J/kg-K)
D diameter (m)
G mass flux (kg/m^{2}s)
h heat transfer coefficient (W/m^{2}K)
M molecular weight (dimensionless)
MBE mean bias error ($= \frac{1}{n}\sum_{i=1}^{n}\frac{h_{ev,calculated}-h_{ev,experimental}}{h_{ev,experimental}}$)
q heat flux (kW/m^2)
Re_f liquid Reynolds number ($= \frac{G(1-x)D}{\mu_l}$, dimensionless)
RMSE root mean square error
($= \sqrt{\frac{1}{n}\sum_{i=1}^{n}\left[\frac{h_{ev,calculated}-h_{ev,experimental}}{h_{ev,experimental}}\right]^2}$)
T temperature (^{o}C)
x vapor quality (dimensionless)

Greek letters

μ dynamic viscosity (Pa-s)
ρ density (kg/m^3)
σ surface tension (N/m)
Δ differential

Subscripts

avg average
C critical
ev evaporative
f frictional
fg latent quantity
g vapor phase
i inlet
l liquid phase
o exit
IA intermittent to annular flow transition
Sat saturation
TP two phase
w wall

Introduction

Environmental issues associated with the enormous use of refrigerants in refrigeration, air conditioning and heat pump industries are now the most woeful thought to the researchers to deal with new fluids to replace the highly used hydroclorofluorocarbons such as R22 due to the proscription imposed by the international amendments and protocols [1,2]. Besides a very interactive thermodynamic qualities, R22 has a large pressure drop in the evaporator and condenser [3] and cause greenhouse gas emissions, which in turn, contribute significantly to the Total Equivalent Warming Impact [TEWI]. One effective solution to reduce this type of greenhouse gas emissions is using eco-friendly and energy efficient refrigerants [4]; isobutane (R600a) as a pure refrigerant, and R410A as a quasi-azeotropic blend (general properties of these refrigerants have been shown in Table 1 [5]) are those belonging to the first rate choices according to the Atmospheric Research and Environment Program (AREP). With a temperature glide, the concentration gradient near the liquid-vapor inter phase causes heat transfer degradation for refrigerant mixture [6]; but the cycle efficiency can be improved [7] by lessening the mean temperature differences between the refrigerant and heat transfer fluid when the mixture is used as the working fluid. Hydrocarbon (R600a), has flammability problems[8], can be a comparable solution to R22 replacement in thermal performances [9] with great environmental aspect. R410A is a near-azeotroic blend, perform better in refrigerant cycle [10] than R22 with a lower pressure loss in the heat exchanger [11].

Two-phase flow heat transfer characteristics plays an important role in designing highly efficient refrigeration and air conditioning unit. The best way to enhance the heat transfer coefficient inside a tube is lowering the tube inner diameter; indeed, the associated pressure drop may cause a larger initial and running cost [12]. It is, thus, very important to grow the accurate quantified knowledge of the heat transfer characteristics and pressure drop variation in a smooth horizontal small tube, even with the new refrigerants and refrigerant mixtures replacement to R22. Moreover, the flow pattern transition in an evaporator tube is also an important factor as the heat transfer phenomena keep changing with the flow regimes along the evaporator tube [13]. A recent review [4] sketched the different theoretical and experimental studies carried out around the globe with the environmentally friendly refrigerant and refrigerant mixtures. Boiling flow characteristics of different refrigerants and their mixtures in smooth tubes have been experimentally investigated by several researchers [6, 7, 9-11, 14-20] over the few decades. But the comprehensive exposure on the heat transfer coefficient and pressure drop with the description of the flow pattern map over the mass flux range for the refrigerants aforesaid, and their performance comparison is really scarce.

Present study analyzes the experimental results of flow boiling heat transfer coefficient and two-phase pressure drop gradient of R600a and R410A inside a smooth circular copper tube of inside diameter 7 mm varying the heat flux in the range of 3-10 kW/m^2; mass flux within the range of 100-400 kg/m^{2}s; the inlet temperature of the evaporator within the range of 5^{o}C-9^{o}C. The objectives of the present study are to develop an accurate flow boiling heat transfer and pressure drop database for important new refrigerants and to provide data to the refrigeration industry for the design of highly efficient evaporators, and to investigate the influence of imposing heat flux, refrigerant mass flux, and vapor quality on the flow boiling characteristics.

1.EXPERIMENTAL APPARATUS AND TEST PROCEDURE:

Figure 1 shows the simplified schematic diagram of the experimental facility to provide the two phase heat transfer phenomena during flow boiling of the test refrigerants under different ranges of test parameters described in Table 2. The test arrangement and test procedure were same as that of the previous work of the author [21].

The test section of 1.2 m effective length was prepared of the smooth copper tube with inner diameter of 7 mm and outside diameter 9.52 mm. The photographic view of the present test section has been depicted in Figure 2. The outside tube wall temperatures were measured by T-type copper-constantan thermocouples at five axial positions, including inlet and exit to the test evaporator tube. At each section, the temperatures were measured at the top, two sides of the middle and bottom of the tube. The average of these temperatures indicates the local wall temperatures. The local saturation pressures at the inlet and outlet of the test evaporator were measured by piezoelectric pressure transducers. The average of these two pressures indicates the saturation pressure at test section and the difference specifies the corresponding pressure drop. The test evaporator tube was heated by flexible Nichrome

Table 1: General properties of refrigerants.

Refrigerant	Constituents	P_C (kPa)	Safety	ODP*	GWP$^\lambda$	Life (yr.)	M
R22 Chlorodifluoromethane	$CHClF_2$	4990	A1	0.05	1810	12	86.466
R600a Isobutane	$CH(CH_3)_2CH_3$	3648	A3	0	4	12±3	58.123
R410A Puron	CH_2F_2 /C_2HF_5 (1:1)	4860	A1	0	2088	16.95	72.58

*Ozone Depletion Potential; $^\lambda$Global Warming Potential.

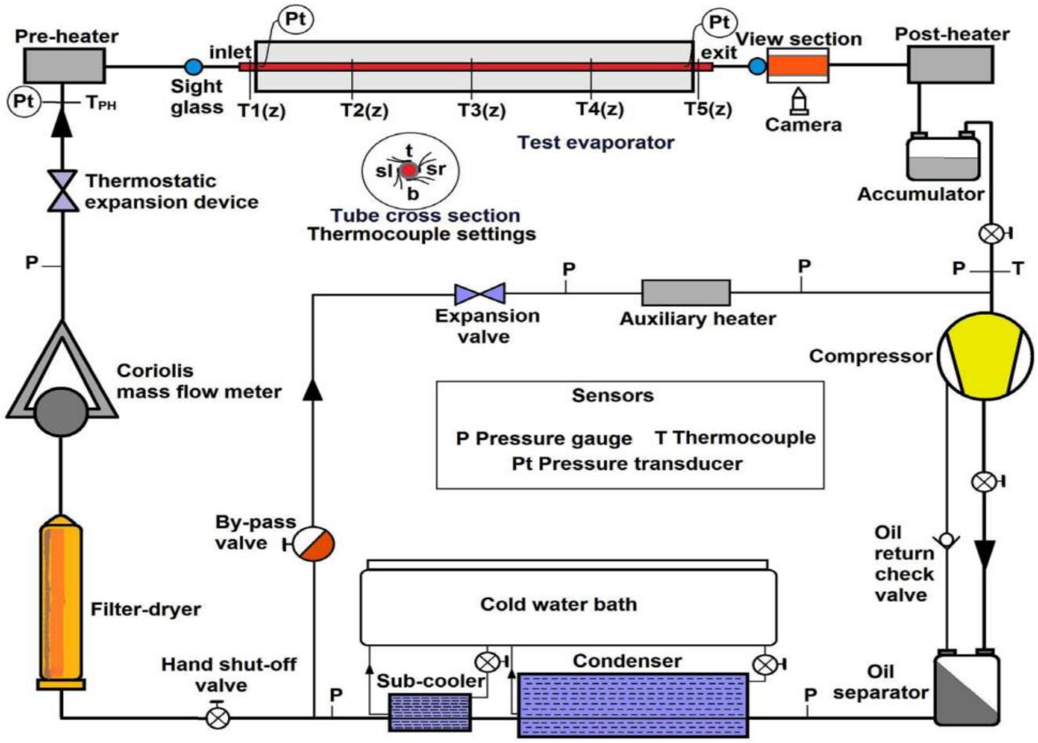

Figure 1: Schematic of test arrangement.

(Nickel-Chromium 80-20 percent by weight) heater wire (3.2 kW capacity at 8m length, with calibrated accuracy of 2W) wrapped over the full test length.

Heat flow to the heater was determined by the current flow and voltage drop across the heater measured by standard clamp meter. The refrigerant flow patterns were observed through the sight glasses installed before the evaporator and captured through a view section with high speed camera installed after the evaporator. To calculate the enthalpy at the entry to pre-heater, another pressure transducer and T-type thermocouples were fitted at a section just prior to the pre-heater. The evaporator tube and heaters were well insulated with glass wool from outside to ensure adiabatic condition. Table 3 shows the features of the plant instrumentation. The temperature and pressure measurement were recorded through a data acquisition system (sampling rate of 0.1-0.2 Hz; 250 kS/s) to store acquired test data to a personal computer. For proper measurement and data acquisition, the test section was connected to earth.

2. DATA ACQUISITION AND DATA REDUCTION:

The 'quasi-local' heat transfer coefficient was calculated by using following Equation (1):

$$\mathrm{h_{ev}} = \left[\frac{\pi \mathrm{D_i} \mathrm{L}\left(\mathrm{T_{w_o}} - \mathrm{T_{Sat}}\right)}{\mathrm{Q}} - \frac{\mathrm{D_i}}{2}\left(\frac{ln[\mathrm{D_o}/\mathrm{D_i}]}{k}\right)\right]^{-1} \quad (1)$$

This is simply based on heat generation by electrical resistance heating of heater wire outside evaporator tube wall and conduction heat flow through the tube wall to the refrigerant flowing inside at steady state condition. The assumptions behind the calculation of

Table 2: Range of test parameters.

Parameters	Range
Refrigerant mass flux	100-400 kg/m^{2}s
Heat flux	3-10 kW/m^2
Vapor quality	0.1-0.9
Inlet temperature	5^{o}C to 9^{o}C

the heat transfer coefficients are same as considered by Copetti et al. [21]. The outside tube wall temperature, T_{w_o}, is the mean of outside wall temperature at the top, two sides of the middle and bottom of the tube at each section in the test evaporator as:

$$T_{w_o} = \frac{T_t(z) + T_{sl}(z) + T_{sr}(z) + T_b(z)}{4} \quad (2)$$

T_{Sat} is the saturation temperature for the pressure readings of the mean of the dew and bubble point temperature for refrigerant mixtures. To evaluate the heat loss to the ambient in the test section and pre-heater, single phase tests were carried out to find the heating coefficient, η defined as the ratio between the output power and input power. η (typically around 0.935) was experimentally determined using the method proposed by Copetti et al. [21].

The resistance heat flow, Q to the refrigerant from outside of the tube (pre-heater and test section) has been calculated by using following Equation (3):

$$Q = \eta \cdot V \cdot I \quad (3)$$

Average vapor quality is calculated by following Equation (4):

$$x_{avg} = (x_i + x_o)/2 \quad (4)$$

where, x_{in} is the inlet dryness fraction of refrigerant to the test section, which is calculated by following Equation (5):

$$x_i = \frac{h_i - h_{f,i}}{h_{fg,i}} \quad (5)$$

h_{in} is the specific enthalpy of the refrigerant at the entry to the test section and the outlet of the pre-heater, which is determined by Equation (6) applying an energy balance on the pre-heater:

$$h_i = h_1 + {Q_{PH}}/{\dot{m}} \quad (6)$$

Enthalpy h_1 is found with respect to the measured temperature and pressure at the entry to the pre-heater and h_{fg} is the latent heat of vaporization of the refrigerant. x_o is the exit dryness fraction of refrigerant from test section can be determined from Equation (7):

$$x_o = \frac{h_o - h_{f,o}}{h_{fg,o}} \quad (7)$$

h_{out} is the exit enthalpy of the refrigerant is determined by applying an energy balance on the test section as:

$$h_o = h_i + {Q_{TS}}/{\dot{m}} \quad (8)$$

The thermodynamic properties of refrigerants were found from REFPROP version 8.0 [22].

The Pressure drop gradient has been calculated from direct difference in pressure readings in the pressure transducers fitted at the inlet and exit of the test evaporator, assuming the pressure drop from the saturation point to the outlet of the test evaporator is a linear function of the tube effective length [21].

The error in measurement depends on the operating conditions and mostly on the accuracy of the wall temperature difference. The experimental uncertainty analysis was done by following Equation (9) proposed by Moffat [23]:

$$U_R = \sqrt{\sum_{i=1}^{N} \left(\frac{\partial R}{\partial V_i} U_{V_i}\right)^2} \quad (9)$$

Where U_R is the estimated uncertainty in calculating the value of desired variable R, due to the independent uncertainty U_{V_i} in the primary measurement of N number of variables V_i, affecting the result. To evaluate the heat loss to the ambient in the test section and pre-heater, single phase tests were carried out to find the heating coefficient, η defined as the ratio between the output power and input power. η (typically around 0.928, shown in

Table 3: Instruments and appliances.

Quantity	**Apparatus**	**Range**	**Accuracy**
Temperature	T-type thermocouple	-50°C to 250°C	±0.2°C
Pressure	Piezoelectric transducers	0 to 20 bar	±0.5% F.S.
Mass flow rate	Coriolis effect mass flow meter	0 to 200 kg/hr	±0.2%
Voltage	AC variable voltage controller	0 to 220 V	±0.5%
Current	Clamp meter	0 to 100 A	±1.0% F.S.±5digits

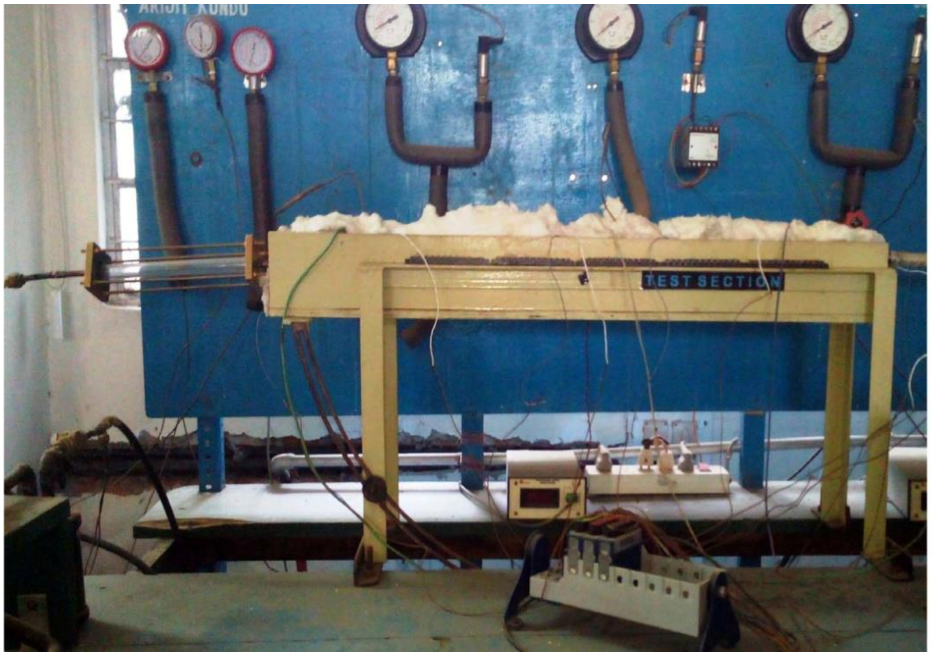

Figure 2: Photographic view of the test section.

Table 4) was experimentally determined using the method proposed by Copetti et al. [22].

The thermodynamic properties of refrigerants were found from REFPROP version 8.0 [23]. The two-phase pressure drop gradient has been calculated from direct difference in pressure readings in the pressure transducers fitted at the inlet and exit of the test evaporator, assuming the pressure drop from the saturation point to the outlet of the test evaporator is a linear function of the tube effective length [22].For evaluating two-phase friction friction factor, the process discussed in our previous paper [24] has been followed.

3. EXPERIMENTAL RESULTS:

In the present paper, the heat transfer coefficients for flow boiling through a horizontal smooth tube are evaluated for two refrigerants; pure fluid R600a, and near-azeotropic blend R410A, by varying the heat flux with different evaporating pressures and mass fluxes while maintaining the refrigerant inlet temperature to the test evaporator between 5^{o}C to 9^{o}C. The experimental conditions are summarized in Table 5. A detailed discussion of the dependence on each operating parameter has been presented in the following subsections.

A. VALIDATION:

In order to establish the integrity of the experimental set-up and verify the temperature and pressure measurements in the present test arrangement, preliminary tests have been performed with R410A,in the single (liquid) phase with the turbulent flow regime. The liquid phase heat transfer coefficients are evaluated and compared with those obtained with the renowned Dittus-Boelter correlations [25]. The experimental heat transfer coefficients show a maximum mean deviation (MD) of 9% (Figure 3).The two-phase flow heat transfer results of the flow boiling of refrigerants through the test evaporator tube are compared with the predicted values by the Liu and Winterton [26], Gungor and Winterton [27], Kandlikar [28], Fang [29] and Mahmoud and Karayiannis [30] correlations has been depicted in Figure 4 and 5.

This confirms that the experimental results on two-phase flow and flow evaporation using the test facility and measurement systems are reliable. The

Table 4: Values of heat coefficient.

Power$_i$ (W)	24.9	73.6	167.2	278.7	328.1	541.8	733.7
Power$_o$ (W)	23.4	66.9	152.5	256.8	309.0	507.1	690.5
η (%)	93.9	90.8	91.2	92.1	94.1	93.6	94.1

Table 5. Operating test conditions.

Fluid		G	q	Δx	Fluid		G	q	Δx
R410A	P_{ev}=9.5 bar	99.6	3.10	0.819-0.138	R600a	P_{ev}=1.91 bar	100.1	3.06	0.879-0.140
		100.4	4.51	0.833-0.128			101.0	4.48	0.843-0.126
		101.0	6.01	0.863-0.140			100.8	6.10	0.863-0.138
		98.8	8.23	0.849-0.127			99.2	7.78	0.845-0.135
		100.2	9.87	0.852-0.138			100.9	10.0	0.828-0.133
	P_{ev}=10.1 bar	199.3	2.97	0.875-0.134		P_{ev}=2.04 bar	201.1	2.98	0.893-0.148
		202.1	4.60	0.871-0.129			200.5	4.97	0.804-0.133
		198.5	5.99	0.889-0.135			200.2	5.89	0.848-0.140
		201.8	8.01	0.864-0.140			198.9	8.11	0.924-0.144
		197.8	9.72	0.888-0.128			198.8	10.2	0.874-0.135
	P_{ev}=10.6 bar	300.6	3.21	0.906-0.149		P_{ev}=2.15 bar	299.6	3.01	0.883-0.136
		301.0	4.50	0.876-0.136			301.3	4.90	0.889-0.130
		298.5	6.08	0.846-0.136			300.2	6.11	0.888-0.121
		301.8	8.13	0.900-0.150			302.8	7.93	0.904-0.140
		299.9	10.1	0.898-0.128			298.9	9.91	0.887-0.132
	P_{ev}=11.9 bar	400.1	3.01	0.887-0.132		P_{ev}=2.47 bar	400.5	3.10	0.895-0.133
		401.0	4.48	0.889-0.130			399.2	5.08	0.868-0.129
		398.3	6.13	0.896-0.122			400.1	6.23	0.896-0.122
		400.8	7.99	0.874-0.135			398.8	8.09	0.866-0.134
		399.5	10.2	0.878-0.130			398.5	9.89	0.881-0.129

experimental result shows the comparison for R600a with an MBE ranging from -12.72% to 156.62% and an RMSE of 20.23 to 283.47%; for R410A with MBE of -20.99% to 207.82% and RMSE of 24.2% to 236.97%, respectively. Among them, the deviations are the smallest by using Liu and Winterton's correlation [26] for R600a, and Gungor-Winterton correlation [27] for R410A.

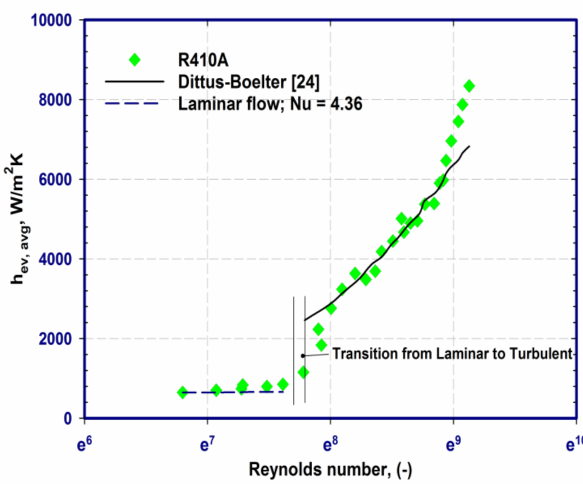

Figure 3. Single phase heat transfer coefficient of R410A.

B. FLOW VISUALIZATION AND FLOW PATTERN MAP:

Flow boiling visualization of test refrigerants under non-adiabatic environment has been carried out on the high tempered borosilicate transparent view

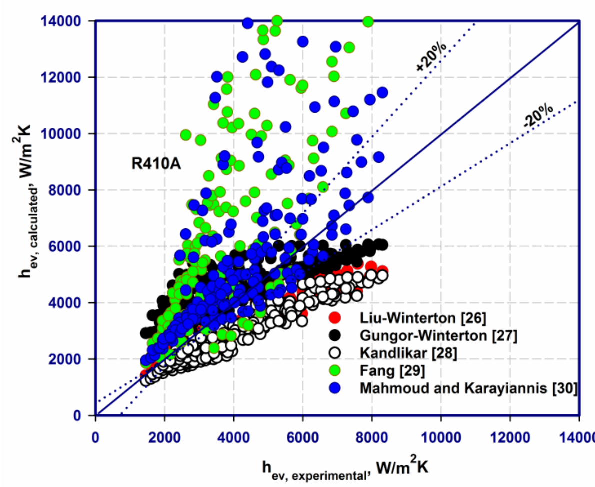

Figure 4. Comparison of R410A results with correlations.

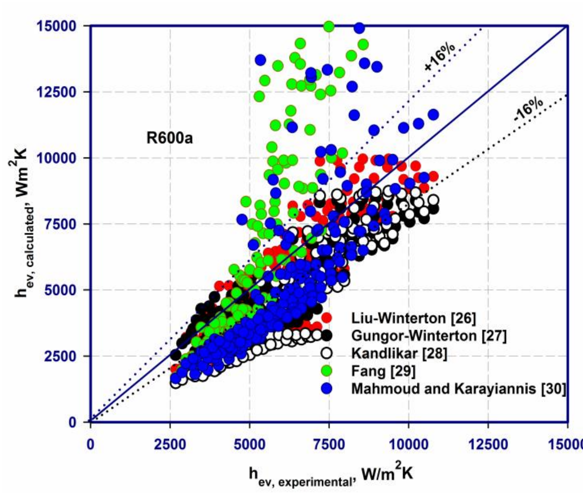

Figure 5.Comparison of R600a results with correlations.

section integrated just after the test evaporator tube. All experiments were executed by altering the imposed heat flux and average vapor quality, while refrigerant mass flux, inlet temperature and inlet pressure were held constant. Several such testings were performed successively varying the mass flux, and pressure.

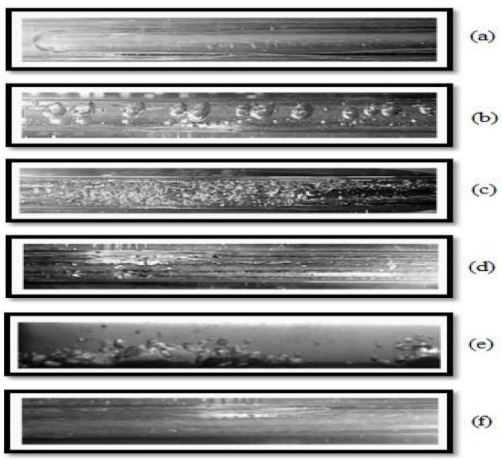

Figure 6: Photographs of flow patterns observed: (a) Slug; (b) Slug to Intermittent; (c) Intermittent; (d) Annular; (e) Stratified-Wavy; (f) Annular with partial Dry-out.

Flow patterns were supervised with a high speed video camera and some stills were captured using a flash synchronized digital camera under steady state conditions. The categorization of flow patterns in circular channels is not yet uni-versally agreed. Nevertheless, the researchers seem to concur to assort their explanation of basic five main flow patterns: bubbly/stratified flow, slug flow, intermittent flow, annular flow and mist flow and each class would be separated into sub-classes. In the present study, the distinct flow patterns identified from the experimental flow visualizations under the test parametric observations were slug flow, inter-mittent flow, slug to intermittent flow, stratified-wavy flow, annular flow and annular with partial dry-out (Figure 6).These patterns correspond to the more commonly detected flow patterns for the exacting test parameters. However, more than a single type of the flow patterns proceeded intermittently in several cases.

The latest version of the flow pattern map of Wojtan et al. [31, 32] is used for the evaluation of two phase flow regimes. Since, the heat transfer process depends upon the flow pattern; one must distinguish the flow pattern regimes during the flow boiling experiments as shown in Figure 7 and 8 for the present study with different test fluids. The flow regimes' identification criteria are the same as used in Mastrullo et al. [33]. These maps provide the transition boundaries (calculated from their under-lying transition equations, as described in Appendix A) on a linear relationship of mass flux versus vapor quality for the particular refrigerant.With increasing gas void fraction, the propinquity of the vapor bub-bles is very close to one another such that bubbles collide and conflate together to form larger bubbles, which are similar to the tube inner diameter and surrounded by a large amplitude liquid wave between them and the tube wall, at the initial stage of the evaporation inside the evaporator tube, recognized as the slug flow regime. The intermittent flow regime is characterized by a large amplitude liquid wave intermittently washing the top of the tube with less amplitude waves in between. Large amplitude liquid contains dispersed small vapor bubbles uniformly with more turbulent vapor-liquid interface than in the slug flow regime, causing strong interaction between the two phases. A stratified wavy flow regime exists, in which the amplitude of the liquid waves is distinguished, but their crests do not reach the top of the tube; only climb up the side wall, leaving thin films of liquid on the tube wall. At a higher gas flow rate, in the annular flow regime, the vapor phase flows in the center of the channel, while the liquid forms a continuous annular film surrounding of the vapor core around the tube perimeter. The dry-out region is severed by a sharp drop in the heat transfer coefficient at a higher vapor quality after it reaches a maximum in the annular zone.Mist flow and stratified flow regimes were not

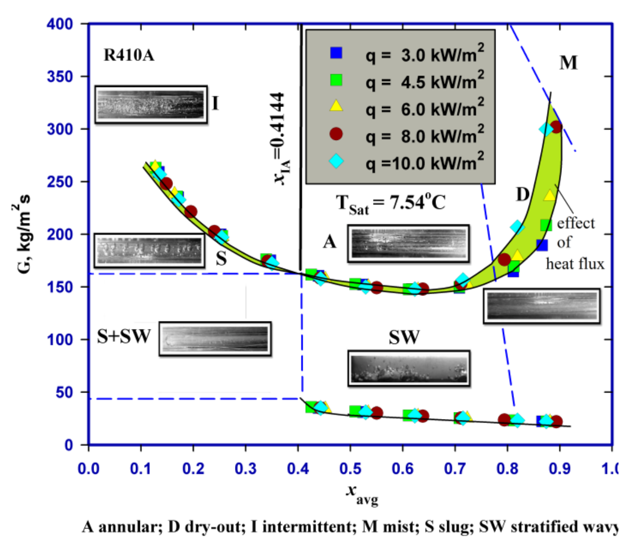

Figure 7: Flow pattern map for R410A.

ascertained within the present range of experiments.

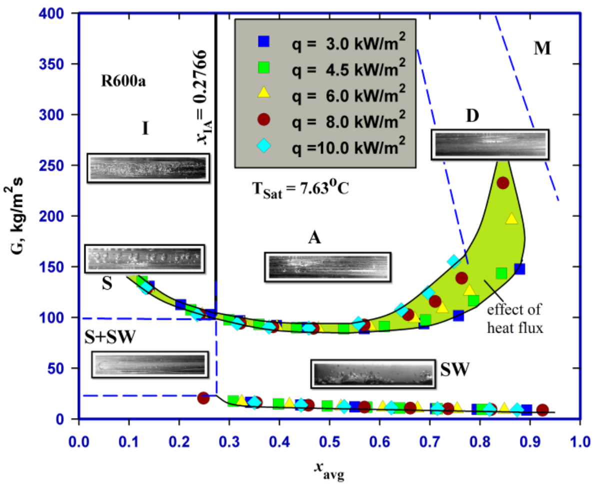

A annular; D dry-out; I intermittent; M mist; S slug; SW stratified wavy.

Figure 8: Flow pattern map for R600a.

The effect of heat flux has been shown on each plot by distinct continuous curve; whereas the broken line shows the distinguished flow pattern zones. The boundary between the annular and stratified-wavy flow regime is dependent on heat flux for R600a (Figure 8); the same for R410Aisto some extent independent of heat flux for $x < 0.7$ (Figure 7), which agrees with the remarks given by Colombo et al. [13]. Intermittent to annular flow pattern transition for R410A has much delayed (with a larger vapor quality) and the transition from annular to wavy flow at respectively lower mass velocities than R600a for nearly the same saturation temperature, as can be seen from these plots. Transition from stratified to wavy region is independent of heat flux, as revealed from the maps.

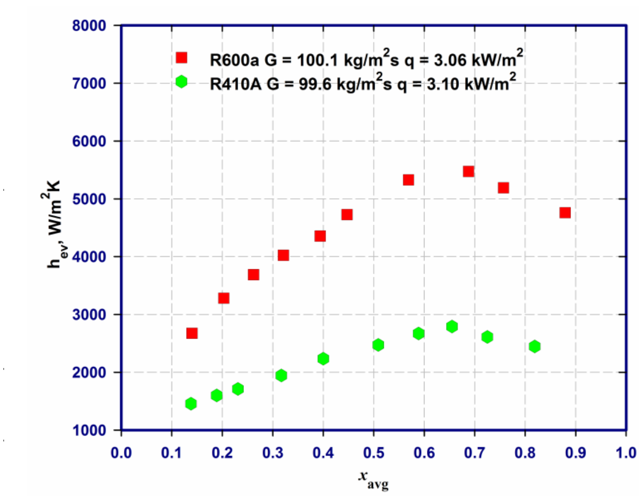

Figure 9: Heat transfer coefficients at nearly constant mass flux of 100 kg/m²s and heat flux of 3 kW/m².

(depending on mass flux) until the occurrence of dry-out. In all cases, the heat transfer coefficients suddenly drop when the liquid film disappears (for high vapor qualities), leaving the tube wall partially or totally dry. The heat transfer coefficients in flow evaporation consequence from the interaction between nucleate boiling and liquid convection. At vapor qualities lower than 0.25, where the slug flow regime has been found, the local heat transfer coefficients of R600a are generally quite sharply increasing, suggesting that at low vapor qualities the nucleate boiling contribution is not negligible for R600a. In the experimental tests where liquid convection is the main mechanism, the heat transfer coefficient increases with quality. Indeed, as the flow proceeds downstream and vaporization takes place, the void fraction increases, thus decreasing the

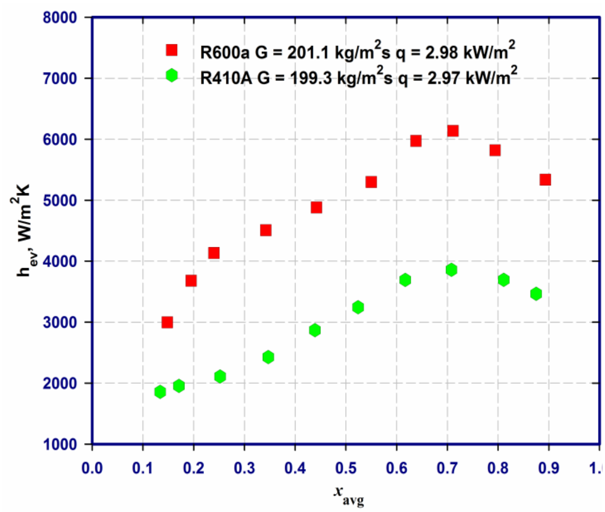

Figure 10: Heat transfer coefficients at nearly constant mass flux of 200 kg/m²s and heat flux of 3 kW/m².

density of the liquid-vapor mixture. As a result, the flow accelerates enhancing convective transport from the heated wall of the tube. The consequent increase in heat transfer coefficient proceeds until the liquid film disappears, leaving the tube wall partially or totally dry. In this region, the heat transfer coefficient decreases because of the low thermal conductivity of the vapor. In the evaporation process where liquid convection is the main mechanism, convective evaporation being predominant does not implicate that nucleate boiling is entirely inhibited. Under these conditions, the heat transfer coefficient increases with vapor quality as explained by Greco and Vanoli [16]. The present study also provides the same occurrence as shown in Figures. (9-11); the increment with respect to that at the inlet of the test evaporator for R600a and R410A is quite high as up to 105% and 123%, respectively, more with respect to the heat transfer coefficient at very low vapor qualities in the range of 0.1 to 0.3 depending on heat fluxes.Due to a temperature glide and variation of the properties of the different constituents inside the near-azeotropic refrigerant mixture R410A (mixture of R32 and R125) make the propagation of the boiling phenomena different from that of the single component refrigerant R600a. Wang and Chiang [20] described the phenomena as at the lower quality region (early stage of vaporization), more volatile component evaporated faster as ρ_g and $\rho_l$for R32 are lower than R125 at the corresponding saturation temperature; but all have very much higher liquid and vapor phase density than those of R600a. Therefore, the lower mean vapor and liquid phase flux for R410A than R600a may cause a sharp delay in flow pattern transition (can be seen byx_{IA} from Figure 7 and 8); and thus, lower heat transfer coefficientsfor R410A than those of R600a till the refrigerant leaves the evaporator tube.

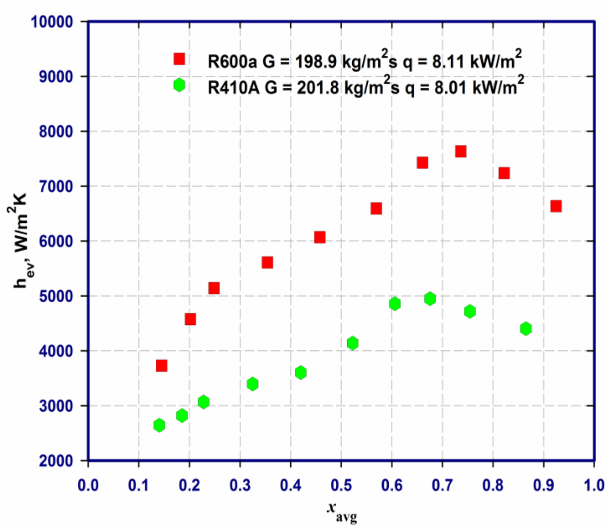

Figure 11: Heat transfer coefficients at nearly constant mass flux of 100 kg/m²s and heat flux of 8 kW/m².

D. EFFECT OF HEAT FLUX ON HEAT TRANSFER COEFFICIENT:

At high heat fluxes, heat transfer is mostly disposed by the nucleate boiling mechanism and the convective contribution to heat transfer predominates at low heat fluxes [15]. The liquid convection contribution can be described by the property combination ψ (shown in Equation 10, according to the Dittus-Boelter [25], single-phase forced convection correlation).

$$\psi = \left(\frac{C_{Pf}}{\mu_f}\right)^{0.4} \cdot k_f^{0.6} \qquad (10)$$

A comprehensive exploration of convective boiling contribution for the test refrigerants reveals that the value of ψ is higher for R600a than R410A at the nearly same saturation temperature. Because of that the heat transfer coefficients of R600a are higher than those of R410A (from Figure 10). From Figure 11 it is clear that when heat flux increases to a high value of 8 kW/m², for the same mass flux, initial difference in the heat transfer coefficients of R600a and R410A decreases; but through the progression of the heat transfer downstream of the evaporator tube, the difference increases by the disposition of the nucleate boiling contribution of the refrigerants. The comparison of average heat transfer coefficients for different test fluids varying the imposed heat flux has been shown in Figure 12. Average heat transfer coefficient, in general, is defined as the mean of local heat transfer coefficients at different vapor qualities for a given imposed heat flux and constant mass flux.

The average heat transfer coefficient trends are depicted by different types of straight lines depending on mass velocities. It is evident from the figure that average heat transfer coefficients increase with the increase in heat fluxes. The increments are more severe at high mass velocities. Also, for each refrigerant, the slope of the line exposes that with increase in heat fluxes, the difference of mean growth increases for the same mass flux condition because of the relative contribution of the nucleate boiling and liquid convection boiling of pure and mixed test fluids in the progression of the boiling

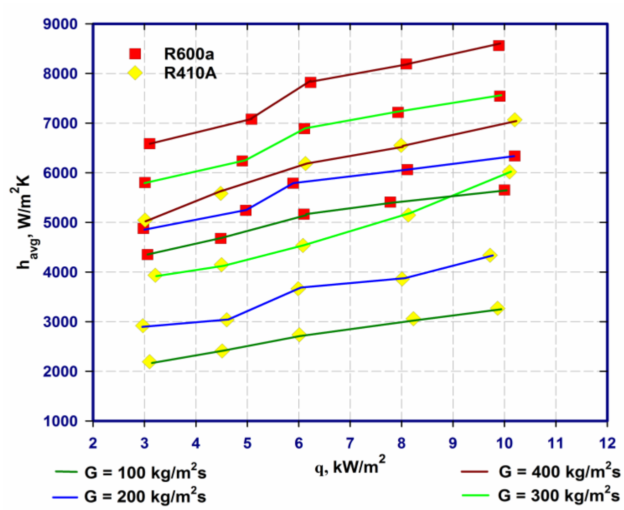

Figure 12: Comparison of average heat transfer coefficients varying heat flux at nearly constant mass velocities.

phenomena through the evaporator tube length. For increases in heat flux from 3 kW/m^2 to 10 kW/m^2, the average heat transfer coefficients of R600a increases in the range of 8-29%; for R410A, it is 10-48%, depending on mass velocities. The average heat transfer coefficients of R600a are about 17-49% more than R410A, depending on mass velocities and heat fluxes; the difference decreases with the increase in mass velocities and heat fluxes.

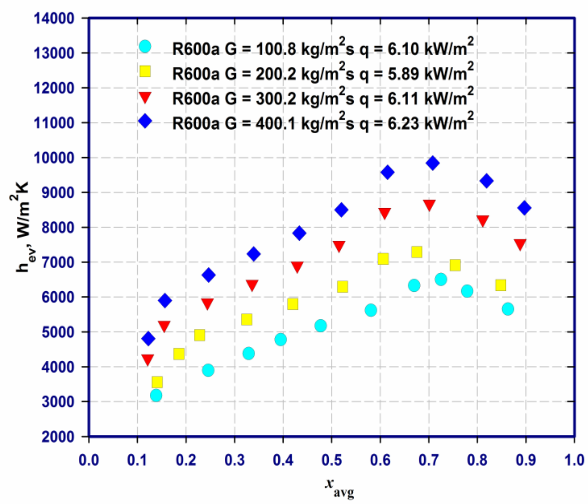

Figure 13: Effect of mass flux on heat transfer coefficients varying vapor quality for R600a.

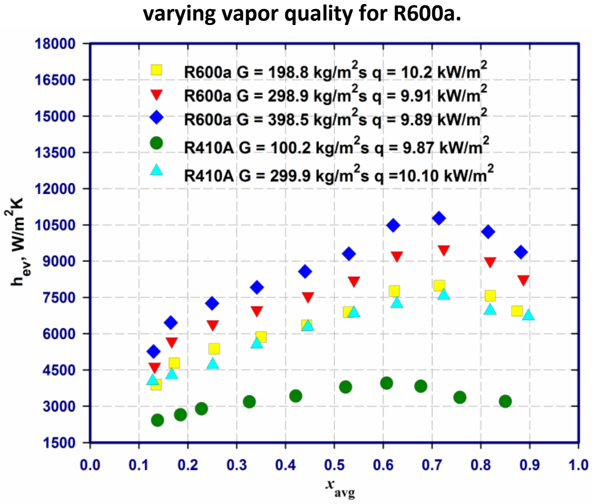

Figure 14: Comparison of heat transfer coefficients varying mass flux at nearly constant heat flux of 10 kW/m^2.

E. EFFECT OF MASS FLUX ON HEAT TRANSFER COEFFICIENT:

At low mass velocities, major contribution to the heat transfer mechanism is the nucleate boiling. As the mass flux increases, the mass transfer resistance to the convective boiling is reduced by the contribution of the more volatile heat transfer coefficient and a higher mass flux induces liquid entrainment to agitate the mass transfer resistance [20]. At the initial stage of the boiling,due to larger contribution of the nucleate boiling part, the heat transfer coefficient increases with enhancing the mass flux for all the refrigerants which can be seen from Figure 13 and 14.

Local boiling heat transfer coefficients of R600a are reported in Figure 13 in order to epitomize the influence of mass flux on heat transfer with a nearly constant heat flux of 6 kW/m^2. In Figure 14, the data compared for all test refrigerants corresponds to an almost constant heat flux of 10kW/m^2 varying the mass flux. The experimental data clearly show that the heat transfer coefficients increase with increasing the refrigerant mass flux. Indeed, increasing the refrigerant mass flux increase the fluid flux, thus enhancing convective boiling. For this eason, as the mass flux increases from 100 to 400 kg/m^{2}s, for the same heat flux applied, heat transfer coefficients of R600a increased far above than those of R410A because of the higher value of property combination ψ with a quite higher active nucleation sites (AN) explaining the nucleate boiling contribution [34] given by Equation 11.

$$AN = \frac{2T_{Sat}\sigma_l}{h_{fg}\rho_g} \tag{11}$$

Here T_{Sat} is the bubble point temperature of refrigerant on corresponding evaporating pressure expressed in Kelvin. In a very low quality region, corresponding to slug flow regimes, where nucleate boiling is dominant, the influence of the refrigerant mass flux is weak and the heat transfer coefficients tend to come together for all the test fluids. The

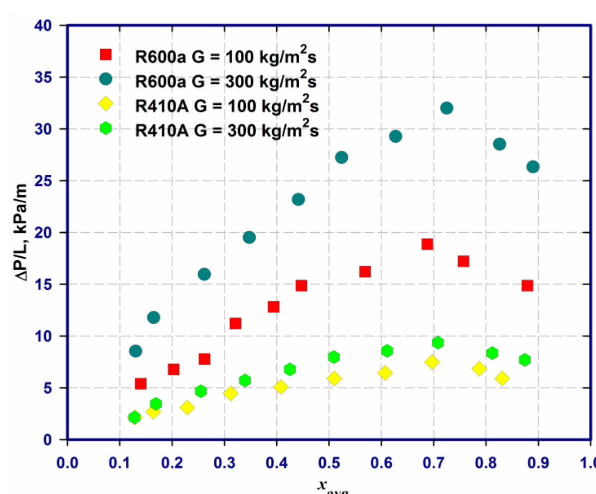

Figure 15: Comparison of pressure drop gradient.

interfacial shear stress is increased by increasing the mass flux, and the bubbles on the heated surface are carried forward from the tube wall under the influence of shear stress and do not attain the larger diameters as seen in pool boiling. This effect results in a reduction in the nucleate boiling component with increasing shear stress, which can be seen from these figures. In these figures, the dependence of the heat transfer coefficients of mass flux is clearly shown. Due to mass transfer resistance, nucleate boiling heat transfer coefficient for refrigerant mixtures with temperature glide are considerably lower than pure refrigerants. From Figure 13, the present study ensures that for increase in mass flux from nearly 100 to 400 kg/m^{2}s, the local heat transfer coefficient of R600a with the heat flux of 6 kW/m^2 increases around 12%-51% before the dry-out starts occurring. About 19%-35% increase in the local heat transfer of R600a occurs for the increment in mass flux from 200 to 400 kg/m^{2}s with heat flux of 10 kW/m^2; and the mass flux increase from 100 to 300 kg/m^{2}s of R410A, h_{ev} increases about 62-97% before the inception of dry-out as can be seen from Figure 14.

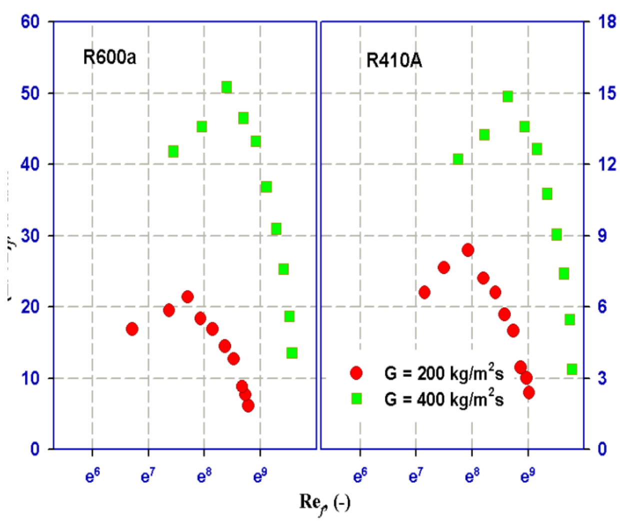

Figure 16: Variation of frictional pressure drop.

F. EFFECT ON PRESSURE DROP:

A highly dependence of the two-phase pressure drop gradient of the refrigerant mass flux and mean vapor quality can be observed in Figure 15. Almost same behavior of the pressure drop variation is present for both the test refrigerants. Indeed, at the low reduced pressures ($P_{reduced}|_{R600a}$ = 0.0526-0.0680; $P_{reduced}|_{R410A}$ = 0.1954-0.2469) the lower ρ_l/ρ_gratio causes a stronger variation of the two-phase density and thus, a large dependence on the mass flux [35] which can be seen from Figure 15. It can be seen that the pressure gradients of all refrigerants confront with the typical acclivity with vapor quality due to the liberal increase of the two-phase mixture flux; then those reach a crest at high vapor qualities and finally fall for each mass flux.

In general, the two-phase pressure drop is primarily sourced by the frictional pressure drop for the horizontal condition of the tube. The variation of two-phase frictional pressure drops of the test refrigerants has been depicted in Figure 16 as a function of liquid Reynolds number. The frictional pressure drop is a change of pressure ensuing from the energy dissipated in the flow by friction, eddying etc. [36]. As the flow goes downstream and vaporization takes place, the density of the liquid-vapor mixture decreases. As a result, the flow accelerates much more and the frictional pressure drops increases. Two-phase frictional pressure drops of R600a are very much higher than those of R410A.The difference increases with the increase in mass flux due to the growth and transition of flow patterns. Considering all the experiments conducted, it can be observed that for the variation of the mass flux from 100 to 300 kg/m^{2}s, the R410A two-phase pressure drops lower by a factor ranging from152%-240%, with respect to those for R600a; where the R600a frictional pressure drops are more than those of R410A in the range of 155%-290% for a change in the mass flux from 200 to 400 kg/m^{2}s.

4. CONCLUSION:

A. Heat transfer coefficient of refrigerants increases with vapor quality. As quality increases, the heat transfer coefficients increase depending on heat flux and mass flux for R600a and R410A up to 105% and 123%, respectively. The heat transfer coefficient then decreases sharply because of dry-out.

B. Heat transfer coefficient of refrigerants depends upon the imposed heat flux.For increase in heat flux from 3 to 10 kW/m^2, the average heat transfer coefficients of R600a increases in the range of 8-29%; for R410A, it is 10-48%, depending on mass velocities.

C. Heat transfer coefficients of pure and mixed refrigerants always increase with mass flux. For the increment in mass flux from 200 to 400 kg/m^{2}s with heat flux of 10 kW/m^2, the local heat transfer coefficients of R600a increase about 19%-35%; and with the mass flux increase from 100 to 300 kg/m^{2}s of R410A, the heat transfer coefficients increase about 62-97% before the inception of dry-out.

D. The average heat transfer coefficients of R600a are about 17-49% more than R410A, depending on mass velocities and heat fluxes; the difference decreases with the increase in mass flux and heat flux.

E. Two-phase pressure drop strongly depends on mass flux and merely on imposing heat flux for all test fluids. For the variation of the mass flux from 200 to400 kg/m^{2}s, R600a frictional pressure drops are more than those of R410A in the range of 155%-290%.

G. Intermittent to annular flow pattern transition for R410A has much delayed and the transition from annular to wavy flow occurs at respectively lower mass velocities than R600a at nearly the same saturation temperature.

Appendix A

Fluid and Geometry Definition

Input: D_i, x_{avg}, T_{sat}, G, q

Physical parameters from REFPROP: ρ_f, ρ_g, μ_f, μ_g, σ, k_f, k_g

Flow Pattern Boundaries Calculation

Stratified to Stratified Wavy transition is calculated from:

$$G_{Stratified} = \left\{\frac{(226.3)^2 A_{fd} A_{gd}^2 \rho_g \left(\rho_f - \rho_g\right) \mu_f g}{x^2(1-x)\pi^3}\right\}^{1/3} \tag{A1}$$

Stratified Wavy to Intermittent /Annular boundary is calculated from:

$$G_{Wavy} = \left\{\frac{16 A_{gd}^3 g D_i \rho_f \rho_g}{x^2\pi^2(1-(2H_{fd}-1)^2)^{0.5}}\left[\frac{\pi^2}{25H_{fd}^2}(1-x)^{-F_1(q)}\left(\frac{We}{Fr}\right)_f^{-F_2(q)}+1\right]\right\}^{1/2} + 50 \tag{A2}$$

Where

$$F_1(q) = 646.0(q/q_C)^2 + 64.8(q/q_C); \qquad F_2(q) = 18.8(q/q_C) + 1.023$$

and $q_C = 0.16\rho_g^{1/2} h_{fg}\left[g\sigma\left(\rho_f - \rho_g\right)\right]^{1/4}$

Intermittent to Annular flow transition is calculated from:

$$x_{IA} = \left\{\left[0.2914\left(\rho_g/\rho_f\right)^{-1/1.75}\left(\mu_f/\mu_g\right)^{-1/7}\right]+1\right\}^{-1} \tag{A3}$$

Annular to Dry-out boundary is calculated from:

$$G_{Dry-out} = \left\{\begin{array}{c}\frac{1}{0.235}\left[\ln\left(\frac{0.58}{x}\right)+0.52\right]\left(\frac{D_i}{\sigma\rho_g}\right)^{-0.17}\cdot \\ \left(\frac{1}{gD_i\rho_g\left(\rho_f-\rho_g\right)}\right)^{-0.37}\cdot\left(\frac{\rho_g}{\rho_f}\right)^{-0.25}\cdot\left(\frac{q}{q_C}\right)^{-0.70}\end{array}\right\}^{0.926} \tag{A4}$$

Dry-out to Mist is calculated from:

$$G_{Mist} = \left\{\begin{array}{c}\frac{1}{0.0058}\left[\ln\left(\frac{0.61}{x}\right)+0.57\right]\left(\frac{D_i}{\sigma\rho_g}\right)^{-0.38}\cdot \\ \left(\frac{1}{gD_i\rho_g\left(\rho_f-\rho_g\right)}\right)^{-0.15}\cdot\left(\frac{\rho_g}{\rho_f}\right)^{-0.09}\cdot\left(\frac{q}{q_C}\right)^{-0.27}\end{array}\right\}^{0.943} \tag{A5}$$

Flow Pattern Classification

Stratified Flow Pattern	$G < G_{strat}$.
Stratified-wavy Flow Pattern	$G > G_{wavy}(x_{IA})$ gives the Slug zone. $G_{strat} < G < G_{wavy}(x_{IA})$ and $x < x_{IA}$ give the Slug/Stratified-Wavy zone.
$x \geq x_{IA}$ gives the Stratified-Wavy zone.	
Intermittent Flow Pattern	$G_{wavy} < G < G_{dry-out}$ and $x < x_{IA}$.
Annular Flow Pattern	$G_{wavy} < G < G_{dry-out}$ and $x > x_{IA}$.
Dry-out Flow Pattern	If $G_{strat} \geq G_{dry-out}$, then $G_{dry-out} = G_{strat}$. If $G_{wavy} \geq G_{dry-out}$, then $G_{dry-out} = G_{wavy}$.
Mist Flow Pattern	If $G_{strat} \geq G_{mist}$, then $G_{mist} = G_{strat}$. If $G_{wavy} \geq G_{mist}$, then $G_{mist} = G_{wavy}$.

REFERENCES:

1. The Copenhagen Amendment. The amendment to the Montreal Protocol agreed by the Fourth Meeting of the Parties (1992). URL http://ozone. unep.org.
2. UNFCCC (United Nations Framework Convention on Climate Change): National Submissions of Greenhouse Gas Emissions on the Common Reporting Format, UNFCCC Secretariat, Bonn, Germany (2003). URL http://unfccc.int.
3. S.J. Smith, L. Shao, S.B. Riffat, Pressure drop of HFC refrigerants inside evaporator and condenser coils as determined by CFD. Appl. Energy 70 (2001) 169-178.
4. M. Mohanraj, S. Jayaraj, C. Muraleedharan, Environment friendly alternatives to halogenated refrigerants-a review. Int. J. Greenhouse Gas Control 3 (2009) 108-119.
5. RefrigerantReport. BitzerInternational, 13thed. 71065 Sindelfingen, Germany (2007). URL http:// www.bitzer.des.
6. D. S. Jung, R.Radermaeher, Prediction of pressure drop during horizontal annular flow boiling of pure and mixed refrigerants. Int. J. Heat Mass Transfer 32(1989) 2435-2446.
7. Kruse, The advantages of non-azeotropic refrigerant mixtures for heat pump application. Int. J. Refrig. 4 (1981) 119-125**.**
8. J.E. Nowacki, Safety with flammable refrigerants, Report No. 7 for NUTEK Program ''Alternative Refrigerants''. Royal Institute of Technology, Applied Thermodynamics and Refrigerants, Stockholm, Sweden (1995).
9. J.Y. Shin, M.S. Kim, S.T. Ro, Experimental study on forced convective boiling heat transfer of pure refrigerants and refrigerant mixtures in a horizontal tube. Int J. Refrig.20 (1997) 267-275.
10. J.T. Oh, A.S. Pamitran, K.I. Choi, P. Hrnjak, Experimental investigation on two-phase flow boiling heat transfer of five refrigerants in horizontal small tubes of 0.5, 1.5 and 3.0 mm inner diameters. Int. J. Heat Mass Transfer 54 (2011) 2080–2088.
11. C.C. Wang, S.K. Chiang, Y.J. Chang, T.W. Chung, Two-phase flow resistance of refrigerants R-22, R-410A and R-407C in small diameter tubes.Trans. IChemE. 79(2001) 553-560.
12. R. Kouhikamali, A.S. Kojidi, M. Asgari, F. Alamolhoda, The effect of condensation and evaporation pressure drop on specific heat transfer surface area and energy consumption in MED-TVC plants. Desalination and Water Treatment 46 (2012) 68-74.
13. L.P.M. Colombo, A. Lucchini, A. Muzzio, Flow patterns, heat transfer and pressure drop for evaporation and condensation of R134A in microfin tubes. Int. J. Refrig. 35 (2012) 2150-2165.
14. D.G. Jung, Mixtures effects on horizontal convective boiling heat transfer. Ph.D. thesis, University of Maryland, College Park, MD(1988) 185.
15. Greco, Convective boiling of pure and mixed refrigerants: An experimental study of the major parameters affecting heat transfer. Int. J. Heat Mass Trans. 51 (2008) 896–909.
16. A. Greco, G.P. Vanoli, Flow-boiling of R22, R134a, R507, R404A and R410A inside a smooth horizontal tube. Int. J. Refrigeration, 28 (2005) 872–880.
17. J.C. Passos, V.F. Kuser, P. Haberschill, M. Lallemand, Convective boiling of R407C inside horizontal micro-fin and plain tubes. Exp. Therm. Fluid Sc. 27 (2003) 705-713.
18. M. Fatouh, A.B. Helali, M.A.M. Hassan, A. Abdala, Heat transfer characteristics of R410A during its evaporation inside horizontal tube.Int.J. Energy Environ. 2 (2011) 701-716.
19. M. Rasti, S.F. Aghamiri, M.S. Hatamipour, Energy efficiency enhancement of a domestic refrigerator usingR436A and R600a as alternative refrigerants to R134a. Int. J. Thermal Sci. 74 (2013) 86-94.
20. C. Wang, C. Chiang, Two phase heat transfer characteristics of R22/R407C in a 6.5-mm smooth tube. Int. J. Heat Fluid Flow 18 (1997) 550-558.
21. Kundu, R. Kumar, A. Gupta,Evaporative heat transfer of R134a and R407C inside a smooth tube with different inclinations. Int. J. Heat Mass Trans. 76 (2014) 523-533.
22. J.B. Copetti, M.H. Macagnan,F. Zinani, N.L.F. Kunsler, Flow boiling heat transfer and pressure drop of R-134a in a mini tube:an experimental investigation. Exp. Therm. Fluid Science 35 (2011) 636-644.
23. E.W. Lemmon, M.L. Huber, M.O. McLinden, Reference fluid thermodynamic and transport properties (REFPROP). version 8.0, in NIST Standard Reference Database 23. Gaithersburg, MD: National Institute of Standards and Technology (2007).

24. A. Kundu, R. Kumar, A. Gupta, Heat transfer characteristics and flow pattern during two-phase flow boiling of R134a and R407C in a horizontal smooth tube. Exp. Therm. Fluid Sci. 57 (2014) 344-352.

25. E.J. Dittus, L.M.K. Boelter, Publications on engineering. Univ. California, Berkeley, 2 (1930) 443.

26. Z. Liu, R.H.S. Winterton, General correlation for saturated and subcooled flow boiling in tubes and annuli, based on a nucleate pool boiling equation. Int. J. Heat Mass Transfer 34 (1991) 2759-2766.

27. K.E. Gungor, R.H.S. Winterton, Simplified general correlation for saturated flow boiling and comparisons of correlations with data. Chem. Eng. Research Design 65 (2) (1987) 148-156.

28. S.G. Kandlikar, A general correlation for saturated two-phase flow boiling heat transfer inside horizontal and vertical tubes. J. Heat Transfer 112 (1990) 219-228.

29. X. Fang, A new correlation of flow boiling heat transfer coefficients based on R134a data. Int. J. Heat Mass Transfer 66 (2013) 279-283.

30. M.M. Mahmouda, T.G. Karayiannis, Heat transfer correlation for flow boiling in small to micro tubes. Int. J. Heat Mass Transfer 66 (2013) 553-574.

31. L. Wojtan, T. Ursenbacher, J.R. Thome, Investigation of flow boilingin horizontal tubes: Part I - A new diabatic two-phase flow patter nmap. Int. J. Heat Mass Transfer 48 (2005) 2955-2969.

32. L. Wojtan, T. Ursenbacher, J.R. Thome, Investigation of flow boilingin horizontal tubes: Part II - Development of a new heat transfer-model for stratified-wavy, dryout and mist flow regimes. Int. J. HeatMass Transfer 48 (2005a) 2970-2985.

33. R. Mastrullo, A.W. Mauro, J.R. Thome, D. Toto, G.P. Vanoli, Flow pattern maps for convective boiling of CO_2 and R410A in a horizontal smooth tube: experiments and new correlations analyzing the effect of the reduced pressure. Int. J. Heat Mass Trans. 55 (2012) 1519-1528.

34. V.P. Carey, Liquid-Vapor Phase Change Pheno-mena. Hemisphere Publishing Corporation, New York; second edition (2007).

35. S. Grauso, R. Mastrullo, A.W. Mauro, J.R. Thome, G.P. Vanoli, Flow pattern map, heat transfer and pressure drops duringevaporation of R-1234ze(E) and R134a in a horizontal, circularsmooth tube: Experiments and assessment of predictive methods. Int. J. Refrig.36(2013)478-491.

36. C. Aprea, A. Greco, A. Rosato, Comparison of R407C and 417A heat transfercoefficients and pressure drops during flow boiling in a horizontal smoothtube. Energy Conv. Manage. 49 (2008) 1629-1636.